This is a preprint, the final version is subject to change, of the American Mineralogist (MSA)
Cite as Authors (Year) Title. American Mineralogist, in press.
(DOI will not work until issue is live.) DOI: http://dx.doi.org/10.2138/am-2016-5619

REVISION 1

SILICIC LUNAR VOLCANISM: TESTING THE CRUSTAL MELTING MODEL

Amber L. Gullikson[1,*], Justin J. Hagerty[2], Mary R. Reid[1], Jennifer F. Rapp[3], David S. Draper[4]

[1]Northern Arizona University, Flagstaff, AZ 86011, USA
[2]U.S. Geological Survey, Astrogeology Science Center, Flagstaff, AZ 86001, USA
[3]Jacobs, NASA Johnson Space Center, Mail Code JE20, Houston, TX 77058, USA
[4]Astromaterials Research office, ARES directorate, NASA Johnson Space Center. Houston, TX, USA
*E-mail: agullikson@usgs.gov

Abstract

Lunar silicic rocks were first identified by granitic fragments found in samples brought to Earth by the Apollo missions, followed by the discovery of silicic domes on the lunar surface through remote sensing. Although these silicic lithologies are thought to make up a small portion of the lunar crust, their presence indicates that lunar crustal evolution is more complex than originally thought. Models currently used to describe the formation of silicic lithologies on the Moon include in-situ differentiation of a magma, magma differentiation with silicate liquid immiscibility, and partial melting of the crust. This study focuses on testing a crustal melting model through partial melting experiments on compositions representing lithologies spatially associated with the silicic domes. The experiments were guided by the results of modeling melting temperatures and residual melt compositions of possible protoliths for lunar silicic rocks using the thermodynamic modeling software, rhyolite-MELTS.

Rhyolite-MELTS simulations predict liquidus temperatures of 950 – 1040 °C for lunar granites under anhydrous conditions, which guided the temperature range for the experiments. Monzogabbro, alkali gabbronorite, and KREEP basalt were identified as potential protoliths due to their ages, locations on the Moon (i.e., located near observed silicic domes), chemically

evolved compositions, and the results from rhyolite-MELTS modeling. Partial melting experiments, using mixtures of reagent grade oxide powders representing bulk rock compositions of these rock types, were carried out at atmospheric pressure over the temperature range of 900 – 1100 °C. Because all lunar granite samples and remotely sensed domes have an elevated abundance of Th, some of the mixtures were doped with Th to observe its partitioning behavior.

Run products show that at temperatures of 1050 and 1100 °C, melts of the three protoliths are not silicic in nature (i.e., they have <63 wt.% SiO_2). By 1000 °C, melts of both monzogabbro and alkali gabbronorite approach the composition of granite, but are also characterized by immiscible Si-rich and Fe-rich liquids. Furthermore, Th strongly partitions into the Fe-rich, and not the Si-rich glass in all experimental runs.

Our work provides important constraints on the mechanism of silicic melt formation on the Moon. The observed high Th content of lunar granite is difficult to explain by silicate liquid immiscibility, because through this process, Th is not fractionated into the Si-rich phase. Results of our experiments and modeling suggests that silicic lunar rocks could be produced from monzogabbro and alkali gabbronorite protoliths by partial melting at T <1000 °C. Additionally, we speculate that at higher pressures (P ≥ 0.005 GPa), the observed immiscibility in the partial melting experiments would be suppressed.

Keywords: Moon, silicic volcanism, crustal melting, partial melting experiments, silicate liquid immiscibility

Introduction

Apart from impact-derived rocks, the Moon's surface is largely made up of both pristine highland rocks, which are divided into two main groups- magnesian suite rocks and ferroan anorthosite, and mare basalt (Warner et al., 1976; Taylor et al., 1991; Papike et al., 1998).

Following Apollo sample-returned missions, small fragments of granites, which are uncommon on the Moon, were identified in several breccia samples (Rutherford et al., 1976; Taylor et al., 1991; Jolliff, 1991). Recently, silica-rich volcanic domes have been identified on the lunar surface (Wood and Head, 1975; Head and McCord, 1978; Jolliff et al., 1999; Chevrel et al., 1999; Wagner et al., 2002; Hawke et al., 2003) and characterized by various remote sensing instruments, such as the Lunar Prospector Gamma Ray Spectrometer, the Diviner Lunar Radiometer Experiment, Lunar Reconnaissance Orbiter imaging and topography (LROC and LOLA), and Clementine Ultraviolet Visible spectrometer (Lawrence et al., 2005; Hagerty et al., 2006; Glotch et al., 2010; Jolliff et al., 2011). Through remote sensing, it was discovered that in addition to silica-rich phases (Glotch et al., 2010), thorium is also abundant in these domes (Lawrence et al., 2005; Hagerty et al., 2006; Glotch et al., 2010).

Three main models have been proposed for the origin of lunar silicic volcanism: in-situ differentiation of a mafic magma, magma differentiation with silicate liquid immiscibility, and crustal melting. In the first model, silicic melts can be produced when basaltic magma stalls in the crust and undergoes extensive crystal-liquid fractionation (e.g., Ryder, 1976; Neal and Taylor, 1989a; Jolliff et al., 2011). Residual melt in the system becomes rich in silica and incompatible trace elements (e.g., Th). There is uncertainty on whether differentiation on its own can achieve the necessary silica enrichment to produce a granitic composition (Jolliff, personal communication). However, if this process did occur on the Moon, a parent magma with elevated concentrations of incompatible trace elements (e.g., a KREEP basalt magma), could have intruded into and ponded in the upper crust, followed by extensive differentiation (Jolliff et al., 2011). This granitic melt will only be a very small fraction of the initial volume of the parent magma.

The second mechanism for the origin of lunar silicic magmas, silicate liquid immiscibility (SLI), is a process wherein the liquid remaining after 90 − 98% crystallization of basaltic magma unmixes into coexisting Fe-rich and Si-rich liquids; if able to separate from its counterpart and coalesce, the Si-rich liquid could crystallize to form granites or rhyolites (Roedder and Weiblen, 1970; Hess, 1989; Jolliff, 1991). This process might be considered a variant of the first mechanism in that the main difference is whether or not the highly differentiated melt produced from the basalt experiences silicate liquid immiscibility. SLI occurred on the Moon on a microscopic scale (Roedder and Weiblen, 1970; Roedder and Weiblen, 1971; Roedder and Weiblen, 1972; Jolliff and Floss, 1997) and has been explored experimentally using both terrestrial and some lunar compositions (e.g., Hess and Rutherford, 1974; Hess et al., 1975; Rutherford et al., 1976; Charlier and Grove, 2012; Charlier et al., 2013). One potential complication for generating lunar silicic rocks this way is that high field-strength cations such as Th preferentially go into the Fe-rich liquid, in apparent contradiction to the observed high abundances of Th present in lunar granites and silicic domes (Hess and Rutherford, 1974; Neal and Taylor, 1989a, Jolliff, 1991; Jolliff, 1998; Shearer et al., 2001; Lawrence et al., 2005; Hagerty et al., 2006). Several studies have discussed the possibility that due to the fractionation of REE-rich whitlockite, hereafter referred to as merrillite, prior to the onset of immiscibility could result in elevated concentrations of Th and other HFS elements in the residual melt (Hess and Rutherford, 1974; Hess et al., 1975; Rutherford et al., 1976; Hess, 1989; Neal and Taylor, 1989a; Jolliff et al., 1991; Jolliff, 1998). It was noted that merrillite has a higher crystal-liquid partition coefficient for La compared to Th and U, and as merrillite crystallizes, the ratios of Th/La and U/La in the residual melt will increase.

The final mechanism that might explain the formation of lunar silicic rocks is the crustal

98 melting model. As heat and volatiles are introduced into the crust by a variety of possible
99 mechanisms (e.g., basaltic underplating), crust can undergo partial melting and silicic rocks can
100 be produced (Figure 1). The crustal melting model explains the formation of a variety of silicic
101 rocks on Earth (e.g., Bergantz, 1989; Annen and Sparks, 2002) and could be considered a likely
102 mechanism in the petrogenesis of these types of rocks on the Moon (Hagerty et al., 2006). One of
103 the main limiting factors for the acceptance of this model is a lack of experimental work
104 simulating the lunar environment, using compositions similar to lunar rocks. Previous partial
105 melting experiments of basaltic rocks have produced silicic melts under a range of different
106 pressures, temperatures, water contents, and oxygen fugacities (R. Rapp et al., 1991; McCarthy
107 and Patiño-Douce, 1997; Koepke et al., 2004; Sisson et al., 2005); such experiments, however,
108 were carried out under terrestrial conditions, using terrestrial compositions.

109 This study focuses on the results of partially melting potential protoliths under lunar
110 conditions to determine whether SLI and/or crustal melting are viable methods for producing
111 lunar granites and rhyolites. Lunar rocks differ from any terrestrial analog, having a distinct
112 chemical composition with low water contents, a lack of hydrous minerals, and typically higher
113 FeO content and lower alkali contents (Goodrich et al., 1986; Heiken et al., 1991; Papike et al.,
114 1998; Jolliff et al., 1999; Bonin, 2002). Such differences might dictate which types of protoliths
115 could undergo partial melting to form lunar granites, as well as require higher melting
116 temperatures because the melting point is not depressed by the presence of H_2O.

117 We hypothesized that monzogabbro, alkali gabbronorite, and KREEP basalt are potential
118 protoliths for lunar granites and rhyolites. These rocks have chemically evolved compositions
119 (e.g. relatively high alkali content and incompatible trace element concentrations), which should
120 result in greater volumes of silicic melt being produced through partial melting at a given

condition when compared to a more primitive composition. Additionally, they have similar ages to lunar granites (4.5 – 3.9 Ga), and have been identified within the Procellarum KREEP Terrane, a region that incorporates the majority of observed silicic domes (Shearer and Papike, 1999; Shervais and McGee, 1999; Jolliff et al., 2000; Wilson and Head, 2003; Hagerty et al., 2006; Wieczorek et al., 2006). Computer simulations of melt equilibria for possible protoliths using rhyolite-MELTS (Gualda et al., 2012; Ghiorso and Gualda, 2015) were used to place constraints on lunar crustal melting temperatures and to test whether the chosen protoliths are likely candidates for the production of lunar granites through cooling simulations.

Details of experimental design

Our experimental work was designed to test both the crustal melting model and the SLI model by crystallization experiments. Although the crustal melting model describes a process wherein rocks are heated and partially melted, when reproduced experimentally, kinetics can be very slow and impede attainment of equilibrium during the experimental run time. We therefore carried out experiments by heating each sample to 1300 °C (above the liquidus), and then cooled them slowly until the target experimental temperature was reached. By doing this, we performed crystallization rather than partial melting experiments. We recognize this is a compromise and this possible complication should be kept in mind when interpreting our results. Because the partitioning of Th between coexisting liquids is particularly important for investigating the robustness of the SLI model for the formation of lunar silicic rocks, starting materials for several of the experiments were also doped with Th.

All crystallization experiments were run at atmospheric pressure, and run temperatures were chosen based on our rhyolite-MELTS modeling results, as well as previous terrestrial partial melting experiments (R. Rapp et al., 1991; McCarthy and Patiño-Douce, 1997).

144 Experiments were carried out at the 1-Bar Gas-Mixing Laboratory at NASA Johnson Space
145 Center (JSC) in Houston, TX. Samples were run in a 1-atm gas-mixing Deltech furnace, held at
146 one log unit below the iron-wüstite (IW) oxygen fugacity (fO_2) buffer (denoted IW-1 hereafter)
147 to simulate the reduced lunar environment (Sato et al., 1973; Bonin, 2002). In this case, fO_2 is
148 controlled by the amount of CO and CO_2 gas that is flowing continuously over the sample. The
149 gas ratio required to hold a fixed fO_2 changes with temperature, so for each experiment the
150 amounts of CO and CO_2 were calculated and adjusted for the specific temperatures. Flow meters
151 for each Deltech furnace are attached to a solid-state zirconia sensor that measures the
152 electromotive force, which is directly related to fO_2 and is used to regulate gas flow over each
153 sample.

154 We approximated the compositions of Apollo samples 14161,7069 (monzogabbro)
155 (Jolliff, 1991), 67975,117 (alkali gabbronorite) (James et al., 1987), and 15386,19 (KREEP
156 basalt) (Warren and Watson, 1978) (Table 1) by using a mixture of powdered oxides and
157 carbonates. Powder mixtures for each lithology were ground together in ethanol using a mortar
158 and pestle to ensure the oxide powders were fully homogenized. Several of the powders used for
159 the starting composition were carbonates (i.e., $CaCO_3$, Na_2CO_3, and K_2CO_3). In order to match
160 starting compositions to lunar material, samples were heated in a box furnace to 800 °C for 2 − 3
161 hours to decarbonate the starting materials. For Th-doped experiments, one milliliter of a 10,000
162 µg/mL thorium solution was added to 2 grams of oxide powder. Samples were doped with much
163 higher amounts of Th (0.5 wt.%) than lunar granite samples (i.e., ~40 – 60 ppm) so that
164 measurements could be made using an electron microprobe. The doped powder was then ground
165 up using a mortar and pestle, dried under a heat lamp, and then ground up an additional time, to
166 ensure Th was dispersed throughout the sample.

Pellets made from each starting material were hung on a rhenium wire loop that was suspended by thicker platinum wires. The platinum wires were attached to an apparatus that allowed samples to be suspended midair in the tube furnace, near the hotspot. Experimental charges were first raised to the target experimental temperature (e.g., 1000 °C), to obtain the correct mixture of CO and CO_2 for the desired fO_2 value. The sample was then heated to 1300 °C and held there for 30 minutes to ensure that the sample had fully melted. The sample was then cooled to the target experimental temperature (e.g., 1000 °C) at a rate of either 5 °C/hr or 30 °C/hr and held for five days before being quenched in water.

Each experimental charge was encased in epoxy, polished, and carbon coated for electron microprobe analysis. Prior to probe analyses, experimental run phases were identified using energy dispersive spectrometry (EDS) on a scanning electron microscope at both JSC and Northern Arizona University (NAU), and back-scattered electron (BSE) images were taken of all the run products. Charges were then analyzed and characterized using wavelength dispersive spectrometry (WDS) at various institutions (NAU, JSC, and University of Arizona (U of A)). Microbeam settings at each institution (i.e., voltage, beam current etc.) are listed in Table 2.

Results

Rationale for experimental design

Textures and mineral compositions of the likely protoliths for lunar silicic lithologies (e.g., monzogabbro, alkali gabbronorite, and KREEP basalt) suggest that they were emplaced at fairly shallow depths, within 1-2 km of the lunar surface, corresponding to a maximum pressure of 0.01 GPa (McCallum and O'Brien, 1996; Jolliff et al., 1999). Because lunar granites and their possible protoliths are nearly anhydrous (Papike et al., 1998; Bonin, 2002) and the apparent pressures of formation are below 0.01 GPa, obtaining experimental results at atmospheric

pressure (i.e., 1 bar) and extrapolating them to the inferred natural pressures of melting was expected to have only minor inaccuracies. All partial melting experiments, therefore, were performed at atmospheric pressure for the sake of experimental simplicity. We subsequently learned that our experiments using monzogabbro and alkali gabbronorite reach the immiscibility field at the lower end of the temperature range explored (i.e. ≤1000 °C), which reflects similar results of previous experimental studies using KREEP basalt and mare basalt compositions, all at atmospheric pressure (Hess et al., 1975; Rutherford et al., 1976).

Experimental protolith compositions and temperatures were guided by the results of thermodynamic phase equilibrium simulations obtained from rhyolite-MELTS (Gualda et al., 2012; Ghiorso and Gualda, 2015). Rhyolite-MELTS is optimized for low-pressure (0-2 GPa) silicic systems where quartz and two feldspars are stabilized. Cooling simulations were applied to monzogabbro, KREEP basalt, and magnesian- and alkali-suite norite and gabbronorite compositions, based on compositions listed in Planetary Materials (Papike et al., 1998). Equilibrium phase assemblages and melt compositions were modeled at temperatures from 900 – 1100 °C and at atmospheric pressure (see supplementary material for details). Three different compositions for each of the four possible lunar protoliths were investigated to determine the most promising starting compositions to use for experiments. Melts of the various rock types were compared to each other and to lunar granite bulk rock compositions (supp. material). Monzogabbro, KREEP basalt, and alkali gabbronorite were identified as target rock types for the experimental study, based on compositions that produced an evolved melt that best matched a lunar granite by 900 °C. Though the residual melt composition of alkali norite resembled lunar granite slightly better than alkali gabbronorite by 900 °C, alkali gabbronorite was chosen for the experimental study due to the volume of liquid that remained in the system. Rhyolite-MELTS

estimated that at 900 °C, alkali norite has ~9 vol% liquid remaining in the system and alkali gabbronorite with 13 vol% (supp. material), causing concern on whether alkali norite would have enough glass for analysis in the experimental runs. Additionally, liquidus temperatures for lunar granites were modeled under a range of pressures (i.e., 0.1, 0.05, and 0.02 GPa) to obtain an upper temperature limit for experiments (Figure 2). Simulations showed that, under anhydrous conditions, temperatures of 1040 °C and lower could be expected to produce granitic melts by partial melting of the protoliths used here.

The accuracy and reliability of the rhyolite-MELTS simulations (Figs. 2 and 3) could be limited by the extent to which they are outside the optimal numerical and experimental range of the model. First, our simulations produced silicic compositions at melt fractions below 50%, whereas rhyolite-MELTS is best suited at >50% liquid (Gualda et al., 2012). Second, both lunar rock compositions and conditions used for our simulations differ from those of the experiments incorporated in rhyolite-MELTS calibration. In general, lunar rocks have higher FeO and lower alkali contents, lower fO_2, and a lack of hydrous minerals compared to terrestrial rocks (Goodrich et al., 1986; Heiken et al., 1991; Papike et al., 1998; Jolliff et al., 1999; Bonin, 2002). Of the rock types used in our simulations, only partial melting and phase equilibria experiments using KREEP basalt and noritic breccias were included in rhyolite-MELTS calibration and the majority of these focused on liquidus phase compositions at high temperatures (e.g., 1150 – 1460 °C) (Walker et al., 1973; Delano, 1977). Thus, while rhyolite-MELTS helped to place important constraints on relevant conditions for crustal melting, partial melting experiments were required to substantiate these and other results.

Experimental glasses

Glass and minerals of sufficient size and quantity for microprobe analysis were produced in crystallization experiments on monzogabbro (1050 and 1000 °C), alkali gabbronorite (1100, 1050, and 1000 °C), and KREEP basalt (1100 °C), and results are presented in Table 3. Monzogabbro and alkali gabbronorite were also crystallized at temperatures of 950 and 900 °C. These experiments were the first to be run in our set and had a much faster cooling rate (i.e., 60 °C/hr) than our higher temperature experiments, which had cooling rates of either 30 °C/hr or 5 °C/hr. The experiments held at 950 and 900 °C produced a quench mat of microcrystalline minerals, resulting in little to no glass available for analysis, and are therefore not discussed further. Experiments run at 1100 and 1050 °C for all protoliths produced glass compositions (even when immiscible) that were more mafic (i.e., <63 wt.% SiO_2) than lunar granites. Only one experiment using KREEP basalt as the starting composition was carried out (i.e., 1100 °C) and due to time constraints, lower temperature experiments were not conducted. Experimental charges held at 1000 °C for both monzogabbro and alkali gabbronorite produced liquids that approach the composition of lunar granites, but also produced compositionally distinct coexisting liquids, one Fe-rich and the other Si-rich. The Si-rich glass obtained for both protoliths matched oxide concentrations in lunar granites for the majority of oxides (Figure 4).

Monzogabbro liquid immiscibility. The onset of immiscibility was observed in the monzogabbro run held at 1050 °C, which produced two different glass compositions that are separated by a diffuse and fuzzy boundary (Figure 5a). The two glasses can be discerned in BSE images: composition 1 is BSE-dark and composition 2 is BSE-bright. The BSE-dark glass (Si-rich glass), located towards the edge of the sample, has an average SiO_2 content of 54 wt.% (Table 3). The BSE-bright glass (Fe-rich glass), which surrounds crystal clusters, has an average

257 SiO_2 value of 48 wt.%. The BSE-bright glass occurs adjacent to phase assemblages which are
258 dominant in plagioclase and a silica polymorph (there are minor amounts of olivine and a Ti-rich
259 oxide as well, totaling <5 vol% of the sample), and is thus enriched in oxides that are
260 incompatible in these minerals (e.g., FeO, TiO_2, and MgO) and depleted in the compatible
261 oxides, SiO_2, Al_2O_3, and Na_2O. The opposite is true for the BSE-dark glass.

262 At 1000 °C, the monzogabbro composition experiment displays immiscible textures
263 (Figure 5b) and is thus fully within the immiscibility field. The experimental run held at this
264 temperature produced Fe-rich and Si-rich glasses separated by a sharp boundary. The Fe-rich
265 glass has 44 wt.% SiO_2 and 23 wt.% FeO, compared to the Si-rich glass, which has 68 wt.% SiO_2
266 and 7 wt.% FeO. The mineral assemblage at this temperature is plagioclase, low-Ca pyroxene, a
267 silica polymorph, Th-rich merrillite, and Ti-rich oxide.

268 Fractionation of Th between coexisting melts was observed for monzogabbro at both
269 investigated temperatures. There are small but resolvable differences in Th concentration
270 between the immiscible liquids at 1050 °C: the Fe-rich glass has 0.87 wt.% Th and the Si-rich
271 glass has 0.64 wt.%, yielding a two-liquid partition coefficient $D(Th)_{mafic/felsic}$ of ~1.4. At 1000
272 °C, the two distinct melts have much larger differences in Th concentration (Fe-rich glass: 2.7
273 wt.%; Si-rich glass: 0.48 wt.%), corresponding to a two-liquid D value of ~5.6.

274 **Alkali gabbronorite liquid immiscibility.** Melts of alkali gabbronorite also fall into the
275 immiscibility field by 1000 °C. Approximately 5% melt remained (comprising both Fe-rich and
276 Si-rich glasses) at this temperature upon quenching. By visible observation using BSE images
277 generated by an electron microprobe, the Si-rich glass is estimated to comprise 80% of the total
278 glass, and the remaining 20% is Fe-rich glass (e.g. Figure 5c). Thorite reached saturation within
279 this system prior to the onset of immiscibility and began crystallizing in this run. The presence of

this mineral, however, does not appear to have affected the overall fractionation trend of Th within the two immiscible glasses. The two-liquid partition coefficient $D(Th)_{mafic/felsic}$ for alkali gabbronorite at 1000 °C is ~12.

The mineral assemblage for alkali gabbronorite at 1050 °C is plagioclase, low-Ca pyroxene, olivine, and thorite. By 1000 °C, this same assemblage occurs, with the addition of ilmenite. One possible caveat that should be mentioned in this experimental series is that phosphorous was not included in the starting composition for alkali gabbronorite, due to the initial study of this rock (James et al., 1987) having no P reported in the bulk composition. There is speculation that up to 2 wt.% P may be present in the rock (Jolliff, personal communication), and if incorporated in the experimental starting composition, it may have resulted in the crystallization of merrillite rather than thorite. Additional experiments would be needed to confirm this idea.

Discussion

The attainment of liquid immiscibility by 1000 °C at atmospheric pressure and the apparent bulk chemical similarity between experimentally produced Si-rich immiscible liquids and lunar silicic rocks, could be interpreted as support for the SLI model. However, the two-liquid partitioning of Th is inconsistent with this model for formation of lunar granite and rhyolites. Our run products show that Th partitions preferentially into the Fe-rich melt (e.g., $D_{mafic/felsic}$ ~5.6 for monzogabbro at 1000 °C). To explain the Th contents of lunar granites (~40 – 60 ppm) and silicic domes (~20 – 70 ppm) (Warren et al., 1987; Morris et al., 1990; Jolliff et al., 1991; Snyder et al., 1992 Lawrence et al., 2005; Hagerty et al., 2006; Jolliff et al., 2011) by SLI at T ≤1000 °C, Fe-rich rocks with exceptionally high Th contents must be present on the Moon (e.g., ≥120 ppm for the Fe-rich endmember, assuming ≥20 ppm in the silicic endmember).

303 Several relatively Fe-rich rocks with elevated Th concentrations have been sampled, for example
304 two monzogabbro fragments were reported to have ~15 wt.% FeO and 37 – 50 ppm Th (Jolliff,
305 1991; Marvin et al., 1991). Though these rocks have comparable Th concentrations to that of
306 lunar granites, no Fe-rich rock has been sampled or detected by remote sensing that has exceeded
307 the amount of Th measured in such granites. Previous studies have discussed the possibility that
308 the crystallization of merrillite prior to immiscibility could increase Th and U concentrations in
309 the residual melt (Hess and Rutherford, 1974; Hess et al., 1975; Rutherford et al., 1976; Hess,
310 1989; Neal and Taylor, 1989a; Jolliff, 1991; Jolliff, 1998). In our monzogabbro experiments,
311 merrillite did not begin to crystallize until after the onset of immiscibility, and therefore Th was
312 not enriched in the melt prior to the two-liquid separation event. This post-SLI merrillite
313 crystallization behavior has also been noted by previous experimental work involving lunar-
314 based compositions (e.g., Longhi, 1990; Rutherford et al., 1996). A hybrid scenario might be
315 possible, wherein evolved liquids produced by partial melting differentiate further by SLI. For
316 SLI to have an appreciable effect, Th contents in the Fe-rich complementary melts would still
317 have to be well in excess of those measured in lunar rocks.

318 Melting at ambient pressure rather than at a slightly elevated pressure was expected to
319 have only minor consequences on solid-liquid equilibria. Liquid immiscibility is, however,
320 enhanced at atmospheric pressure (Rutherford at al., 1996; Charlier et al., 2013). For example,
321 Rutherford et al. (1996) performed a series of experiments using a KREEP basalt composition
322 and showed that at 1-atm the immiscibility field was reached. When the pressure was raised to
323 0.3 GPa, the sample crystallized without reaching the liquid immiscibility field. We predict that
324 at relevant crustal melting conditions (i.e., 0.005 – 0.1 GPa, corresponding to a depth of 1 - 20
325 km), melts like those in our experiments would be present, but would not exsolve to form two

liquids. If so, the weighted mean compositions of the coexisting liquids in our experiments could represent those of partial melts at expected melting conditions (Figure 4).

Alkali gabbronorite produces ~5% melt at 1000 °C and the total weighted mean liquid composition is felsic (67 wt.% SiO_2). At temperatures <1000 °C, it is possible to produce an evolved melt close to a lunar granite using this protolith, though there may only be trace amounts of melt generated at these lower temperatures. The monzogabbro protolith has a weighted mean liquid composition that is intermediate (56 wt.% SiO_2), and produces ~40% melt at 1000 °C. If melting occurred at shallow depths in the crust and the immiscibility field was not reached, it is possible that a residual melt composition similar to that of lunar granite could be produced through partial melting a monzogabbro at temperatures <1000 °C, and still produce a sufficient amount of melt that could become mobile and migrate upwards through the heated material towards the surface.

Although the equilibrium crystallization experiments reported here did not produce melts with granitic compositions solely through crystallization (i.e. felsic melts that were generated in the experiments were the result of immiscibility), general temperature constraints for producing such melts by crustal melting can be inferred. Previous work has estimated that lunar granites should form under temperatures ranging from 900 – 990 °C (Tuttle and Bowen, 1958; Jolliff et al., 1999). This, considered together with our projection that partial melts of a monzogabbro could reach a lunar granite composition at temperatures below 1000 °C at depths where immiscibility does not take place, provides support for the crustal melting model.

Implications

We have experimentally investigated both the lunar crustal melting and the silicate liquid immiscibility models to determine whether one or both are viable mechanisms for producing

349 silicic rocks on the Moon. Our work shows that the lunar crustal melting model is a reasonable
350 candidate for producing lunar granites and rhyolites, and that monzogabbro is the most likely
351 source rock of such melts. However, this hypothesis assumes that at expected melting depths of
352 approximately 1 km, melt compositions would be similar to those obtained in our experiments at
353 atmospheric pressure without the onset of SLI, and finally that in this near surface environment,
354 cooling would be slow enough to allow lunar gravity to cause separation of the silica-rich melt
355 from crystals remaining from the partial melting event. This experimental work has enabled us to
356 estimate Th partitioning between Fe-rich and Si-rich silicate melts. The partitioning behavior of
357 Th is not consistent with SLI being the main mechanism of lunar granite petrogenesis. Our
358 experiments show that Th is much more compatible in Fe-rich melts than in Si-rich melts, which
359 implies that for lunar granites containing up to 20 ppm Th to have formed by SLI, there must be
360 a complementary Fe- and Th-rich reservoir associated with these granites. To date no such
361 reservoir has been observed on the Moon. Silicic lunar magmas are assumed to be generated
362 within the lunar crust at depths of ~1 km, corresponding to a pressure of 0.005 GPa (McCallum
363 and O'Brian, 1996; Jolliff et al., 1999), based on the data from small 1 cm size lunar granite
364 samples. We have shown that at atmospheric pressure immiscible liquids form that are consistent
365 with major oxide concentrations of silicic lunar magmas. Additional experiments at higher
366 pressure (0.005 - 0.1 GPa) are now needed to determine the pressure of the onset of SLI in lunar
367 silicic melts, and to further constrain the crustal melting model.

368 **Acknowledgements**

369 Funding for this work was provided by the Geological Society of America research grant, Sigma
370 Xi Grants-in-Aid Research, the NAU Support for Graduate Students program, and the Tom and
371 Rose Bedwell Earth Physics Scholarship.

References cited

Annen, C., and Sparks, R.S.J. (2002) Effects of repetitive emplacement of basaltic intrusions on thermal evolution and melt generation in the crust, Earth and Planetary Science Letters, 203, 937-955.

Bergantz, G.W. (1989) Underplating and partial melting: Implications for melt generation extraction, Science, 245, no. 4922, 1093-1095.

Blanchard, D.P., and McKay, G.A. (1981) Remnants from the ancient lunar crust III: Norite 78236, Lunar and Planetary Science Conference XII, 83-85.

Blanchard, D.P., Haskin, L.A., Jacobs, J.W., Brannon, J.C., and Korotev, R.L. (1975) Major and trace element chemistry of Boulder 1 at Station 2, Apollo 17, The Moon, 14, 359-371.

Bonin, B., Bébien, J., and Masson, P. (2002) Granite: A planetary point of view, Gondwana Research, 5, no. 2, 261-273.

Charlier, B., and Grove, T.L (2012) Experiments on liquid immiscibility along tholeiitic liquid lines of descent, Contributions to Mineralogy and Petrology, 164, 27-44.

Charlier, B., Namur, O., and Grove, T. (2013) Compositional and kinetic controls on liquid immiscibility in ferrobasalt-rhyolite volcanic and plutonic series, Geochimica et Cosmochimica Acta, 113, 79-93.

Chevrel, S.D., and Pinet, P.C. (1999) Gruithuisen domes region: A candidate for an extended nonmare volcanism unit on the Moon, Journal of Geophysical Research, 104, no. E7, 515-529.

Delano, J.W. (1977) Experimental melting relations of 63545, 76015, and 76055, Proceedings of the Eighth Lunar Science Conference, 2097-2123.

394 Ghiorso, M.S., and Gualda, G.A.R. (2015) An H_2O-CO_2 mixed fluid saturation model
395 compatible with rhyolite-MELTS, Contributions to Mineralogy and Petrology, 2015, in
396 press.
397 Glotch, T.D., Lucey, P.G., Bandfield, J.L., Greenhagen, B.T., Thomas, I.R., Elphic, R.C.,
398 Bowles, N., Wyatt, M.B., Allen, C.C., Hanna, K.D., and Paige, D.A. (2010), Highly
399 Silicic Compositions on the Moon, Science, 329, 1510, doi: 10.1126/science.1192148.
400 Goodrich, C.A., Taylor, G.J., Keil, K., Kallemeyn, G.W., and Warren, P.H. (1986), Alkali norite,
401 troctolites, and VHK mare basalts from breccia 14304, Journal of Geophysical Research,
402 91 (B4), 305-318.
403 Gualda, G.A.R., Ghiorso, M.S., Lemons, R.V., and Carley, T.L. (2012) Rhyolite-MELTS: A
404 modified calibration of MELTS optimized for silicic-rich, fluid-bearing magmatic
405 systems, Journal of Petrology, 53, no. 5, 875-890.
406 Hagerty, J.J., Lawrence, D.J., Hawke, B.R., Vaniman, D.T., Elphic, R.C., and Feldman, W.C.
407 (2006), Refined thorium abundances for lunar red spots: Implications for evolved,
408 nonmare volcanism on the Moon. Journal of Geophysical Research, 111, 1-20.
409 Hawke, B.R., Lawrence, D.J., Blewett, D.T., Lucey, P.G., Smith, G.A., Spudis, P.D., and Taylor,
410 G.J. (2003), Hansteen Alpha: A volcanic construct in the lunar highlands. Journal of
411 Geophysical Research, 108 (E7), 5069, doi: 10.1029/2002JE002013.
412 Head, J.W., and McCord, T.B. (1978) Imbrian-age highland volcanism on the Moon; the
413 Gruithuisen and Mairan domes, Science, 199 (4336), 1433-1436.
414 Heiken, G., Vaniman, D., and French, B.M. (1991) Lunar sourcebook: a user's guide to the
415 Moon, Cambridge University Press.

Hess, P.C. (1989) Highly evolved liquids from the fractionation of mare and nonmare basalts, paper presented at Workshop on the Moon in Transition, LPI Tech Report 89-03, Lunar and Planetary Institute, Houston, TX.

Hess, P.C., and Rutherford, M.J. (1974) Element fractionation between immiscible melts, Lunar Science V, 328-330.

Hess, P.C., Rutherford, M.J., Guillemette, R.N., Ryerson, F.J., and Tuchfeld, H.A. (1975) Residual products of fractional crystallization of lunar magmas: An experimental study, Proceedings of the Sixth Lunar Science Conference, 895-909.

James, O.B., Lindstrom, M.M., and Flohr, M.K. (1987) Petrology and geochemistry of alkali gabbronorite from lunar breccia 67975, Proceedings of the 17th Lunar and Planetary Science Conference in Journal of Geophysical Research, 89, E314-E330.

Jolliff, B.L. (1991) Fragments of quartz monzodiorite and felsite in Apollo 14 soil particles, Proceedings of the 21st Lunar and Planetary Science Conference, 101-118.

Jolliff, B.L. (1998) Large-scale separation of K-frac and REEP-frac in the source regions of Apollo impact-melt breccias and a revised estimate of the KREEP composition, International Geology Review, 10, 916-935.

Jolliff, B.L., and Floss, C. (1997) Liquid immiscibility in a lunar plutonic setting and the evolution of KREEPy residual melts, Lunar and Planetary Science Conference XXVIII, 673-674.

Jolliff, B.L., Haskin, L.A., Colson, R.O., and Wadhwa, M. (1993) Partitioning in REE-saturated minerals: Theory, experiment, and modeling of whitlockite, apatite, and evolution of lunar residual magmas, Geochimica et Cosmochimica Acta, 57, 4069-4094.

438 Jolliff, B.L., Floss, C., McCallum, I.S., and Schwartz, J.M. (1999) Geochemistry, petrology, and
439 cooling history of 14161, 7373: A plutonic lunar sample with textural evidence of
440 granitic-fraction separation by silicate liquid immiscibility, American Mineralogist, 84,
441 821-837.
442 Jolliff, B.L., Gillis, J.J., Haskin, L.A., Korotev, R.L., and Wieczorek, M.A. (2000) Major lunar
443 crustal terranes: Surface expressions and crust-mantle origins, Journal of Geophysical
444 Research, 105, (E2) 4197-4216.
445 Jolliff, B.L., Wiseman, S.A., Lawrence, S.J., Tran, T.N., Robinson, M.S., Sato, H., Hawke, B.R.,
446 Scholten, F., Oberst, J., Hiesinger, H., van der Bogert, C.H., Greenhagen, B.T., Glotch,
447 T.D., and Paige, D.A. (2011) Non-mare silicic volcanism on the lunar farside at
448 Compton-Belkovich, Nature, 4, 566-577.
449 Koepke, J., Feig, S.T., Snow, J., and Freise, M. (2004) Petrogenesis of oceanic plagiogranites by
450 partial melting of gabbros: an experimental study, Contributions to Mineralogy and
451 Petrology, 146, 414-432.
452 Laul, J.C. (1986) Chemistry of the Apollo 12 highland component, Proceedings of the 16th
453 Lunar and Planetary Science Conference, Journal of Geophysical Research, 91, D251-
454 D261.
455 Lawrence, D.J., Hawke, B.R., Hagerty, J.J., Elphic, R.C., Feldman, W.C., Prettyman, T.H., and
456 Vaniman, D.T. (2005) Evidence for a high-Th, evolved lithology on the Moon at
457 Hansteen Alpha, Geophysical Research Letters, 32, doi:10.1029/2004GL022022,2005.
458 Longhi, J. (1990) Silicate liquid immiscibility in isothermal crystallization experiments,
459 Proceedings of the 20th Lunar and Planetary Science Conference, 13-24.

460 Marvin, U.B., Lindstrom, M.M., Holmberg, B.B., and Martinez, R.R. (1991) New observations
461 on the quartz monzodiorite-granite suite, Proceedings of the 21st Lunar and Planetary
462 Science Conference, 119-135.
463 McCallum, I.S., and O'Brien, H.E. (1996) Stratigraphy of the lunar highland crust: Depths of
464 burial of lunar samples from cooling-rate studies, American Mineralogist, 81, 1166-1175.
465 McCarthy, T.C., and Patiño Douce, A.E. (1997) Experimental evidence for high-temperature
466 felsic melts formed during intrusion of the deep crust, Geology, 25, 463-466.
467 Mills, R.D., and Simon, J.I. (2012) Predicting the sources and formation mechanisms of evolved
468 lunar crust by linking K/Ca ratios of lunar granites to analogous terrestrial igneous rocks,
469 Second conference on the lunar highlands crust, no. 9011.
470 Morris, R.W., Taylor, G.J., Newsom, H.E., Keil, K., and Garcia, S.R. (1990) Highly evolved and
471 ultramafic lithologies from Apollo 14 soils, Proceedings of the 20th Lunar and Planetary
472 Science Conference, 61-75.
473 Neal, C. R., and Taylor, L.A. (1989a) The nature of barium partitioning between immiscible
474 melts: A comparison of experimental and natural systems with reference to lunar granite
475 petrogenesis, Proceedings of the 19th Lunar and Planetary Science Conference, 209-218.
476 Papike, J.J., Ryder, G., and Shearer, C.K. (1998) Lunar samples, In Mineralogical Society of
477 America Reviews in Mineralogy, 36, 5-01–5-189.
478 Rapp, R.P., Watson, E.B., and Miller, C.F. (1991) Partial melting of amphibolite/eclogite and the
479 origin of Archean trondhjemites and tonalites, Precambrian Research, 51, 1-25.
480 Roedder, E., and Weiblen, P.W. (1970) Silicate liquid immiscibility found in lunar rocks,
481 Geotimes, 10-13.

Roedder, E., and Weiblen, P.W. (1971) Petrology of silicate melt inclusions. Apollo 11 and Apollo 12 and terrestrial equivalents, Proceedings of the Second Lunar Science Conference, Geochimica et Cosmochimica Acta, Suppl. 2, Volume 1, 507-528. M.I.T. Press.

Roedder E., and Weiblen, P.W. (1972a) Petrographic features and petrologic significance of melt inclusions in Apollo 14 and 15 rocks, Proceedings of the Third Lunar Science Conference, 251-279.

Rutherford, M.J., Hess, P.C., Ryerson, F.J., Campbell, H.W., and Dick, P.A. (1976) The chemistry, origin, and petrogenetic implications of lunar granite and monzonite, Proceedings of the Seventh Lunar Science Conference, 1723-1740.

Rutherford, M.J., Tonks, B., and Holmberg, B. (1996) Experimental study of KREEP basalt evolution: The origin of QMD and granite at the base of the lunar crust, Lunar and Planetary Science XXVII, abstract 1113.

Ryder, G. (1976) Lunar sample 15405: Remnant of a KREEP basalt-granite differentiated pluton, Earth and Planetary Science Letters, 29, 255-268.

Ryder, G., and Sherman, S.B. (1989) The Apollo 15 coarse-fines (4-10 mm), JSC # 24035, NASA Johnson Space Center, Houston.

Ryder, G., and Martinez, R.R. (1991) Evolved hypabyssal rocks from Station 7, Apennine Front, Apollo 15, Proceedings of the 21st Lunar and Science Conference, 137-150.

Sato, M., Hickling, N.L., and McLane, J.E. (1973) Oxygen fugacity values of Apollo 12, 14, and 15 lunar samples and reduced state of lunar magmas, Proceedings of the Fourth Lunar Science Conference, 1061-1079.

504 Seddio, S.M., Jolliff, B.L., Korotev, R.L., and Zeigler, R.A. (2013) Petrology and geochemistry
505 of lunar granite 12032,366-19 and implications for lunar granite petrogenesis, American
506 Mineralogist, 98, 1697-1713.
507 Shearer, C.K., and Papike, J.J. (1999), Magmatic evolution of the Moon, American Mineralogist,
508 84, 1469–1494.
509 Shearer, C.K., Papike, J.J., and Spilde, M.N. (2001) Trace-element partitioning between
510 immiscible lunar melts: An example from naturally occurring lunar melt inclusions,
511 American Mineralogist, 86, 238-246.
512 Shearer, C.K., Hess, P.C., Wieczorek, M.A., Pritchard, M.E., Parmentier, E.M., Borg, L.E.,
513 Longhi, J., Elkins-Tanton, L.T., Neal, C.R., Antonenko, I., Canup, R.M., Halliday, A.N.,
514 Grove, T.L., Hager, B.H., Lee, D-C., and Wiechert, U. (2006) Thermal and magmatic
515 evolution of the Moon, Reviews in Mineralogy and Geochemistry, 60, 365-518.
516 Shervais, J.W., and McGee, J.J. (1999) Petrology of the Western Highland Province: ancient
517 crust formation at the Apollo 14 site, Journal of Geophysical Research, 104, 5891-5920.
518 Sisson, T.W., Ratajeski, K., Hankins, W.B., and Glazner, A.F. (2005) Voluminous granitic
519 magmas from common basaltic sources, Contributions to Mineralogy and Petrology, 148,
520 635-661.
521 Snyder, G.A., Taylor, L.A., Liu, Y-G., and Schmitt, R.A. (1992) Petrogenesis of the western
522 highlands of the Moon: Evidence from a diverse group of whitlockite-rich rocks from Fra
523 Mauro Formation, Proceedings of the 22nd Lunar and Planetary Science Conference,
524 399-416.

525 Taylor, G.J., Warren, P., Ryder, G., Delano, J., Pieters, C., and Lofgren, G. (1991) Lunar rocks.
526 In: Lunar Sourcebook. A user's guide to the Moon. Hieken G.H., D.T. Vaniman, and
527 B.M. French (eds) Cambridge University Press, 183-284.
528 Taylor, S.R., Taylor, G.J., and Taylor, L.A. (2006) The Moon: A Taylor perspective,
529 Geochimica et Cosmochimca Acta, 70, 5904-5918.
530 Tuttle, O.F., and Bowen, N.L. (1958) Origin of granite in the light of experimental studies in the
531 system $NaAlSi_2O_8$-$KAlSi_3O_8$-SiO_2-H_2O, Geological Society of America, 74.
532 Wagner, R.J., Head, J.W., Wolf, U., and Neukum, G. (2002) Stratigraphic sequences and ages of
533 volcanic units in the Gruithuisen region of the Moon, Journal of Geophysical Research,
534 107(E11), 5104, doi: 10,1029/2002JE001844.
535 Walker, D., Grove, T.L., Longhi, J., Stopler, E.M., and Hays, J.F. (1973) Origin of lunar
536 feldspathic rocks, Earth and Planetary Science Letters, 20, 325-336.
537 Warner, J.L., Simonds, C.H., and Phinney, W.C. (1976) Genetic distinction between anorthosites
538 and Mg-rich plutonic rocks: New data from 76255, Lunar and Planetary Science, VII,
539 915-917.
540 Warren, P.H., and Wasson, J.T. (1978) Compositional-petrologic investigation of pristine
541 nonmare rocks. Proceeding of the 9th Lunar and Planetary Science Conference, 185-217.
542 Warren. P.H., Taylor, G.J., Keil. K., Marshall, C., and Wasson, J.T. (1981) Foraging westward
543 for pristine non-mare rocks: Complications for petrogenetic models, Proceedings of the
544 12th Lunar and Planetary Science Conference, 21-40.
545 Warren, P.H., Taylor, G.J., Keil, K., Shirley, D.N., and Wasson, J.T. (1983) Petrology and
546 chemistry of two "large" granite clasts from the Moon, Earth and Planetary Science
547 Letters, 64, 175-185.

548 Warren, P.H., Jerde, E.A., and Kallemeyn, G.W. (1987) Pristine Moon rocks: A "large" felsite
549 and a metal-rich ferroan anorthosite, Proceedings of the 17th Lunar and Planetary
550 Science Conference in Journal of Geophysical Research, 92: E303-E313.
551 Wieczorek, M.A., Neumann. G.A., Nimmo, F., Kiefer, W.S., Taylor, G.J., Melosh, H.J., Phillips,
552 R.J., Solomon, S.C., Andrews-Hanna, J.C., Asmar, S.W., Konopliv, A.S., Lemoine, F.G.,
553 Smith, D.E., Watkins, M.M., Williams, J.G., and Zuber, M.T. (2013) The crust of the
554 Moon as seen by GRAIL, Science, 339, 671-675.
555 Wilson, L., and Head, J.W. (2003), Lunar Gruithuisen and Mairan domes: Rheology and mode
556 of emplacement, Journal of Geophysical Research, 108(E2), 5012,
557 doi:10.1029/2002JE001909.

558 Wood, C.A., and Head, J.W. (1975) Geologic setting and provenance of spectrally distinct pre-
559 mare material of possible volcanic origin, paper presented at Conference on Origin of
560 Mare Basalts, Lunar Sci. Inst., Houston, TX.

561

562 List of figure captions:

563 **Figure 1**. Based on a diagram by Hildreth (1981) and adapted to the lunar crust by Hagerty et al.
564 (2006), this image depicts the formation of silicic rocks through partial melting of the lunar crust.
565 Image shows ponded basalts, located on the rims of large impact basins. On right side granites
566 are produced by partial melting the lunar crust by basaltic underplating, and left side extrusive
567 silica-rich volcanism occurs by similar processes. Used by permission of John Wiley and Sons,
568 from Hagerty et al. (2006), Journal of Geophysical Research, vol. 111, Fig. 8, p. 16.
569
570 **Figure 2.** Variation in liquidus temperature of three lunar granites with water content and
571 pressure as determined using rhyolite-MELTS. Granite sample numbers and bulk rock
572 compositions are listed in the supplementary material. Water contents considered in calculations
573 range in steps from 0.0 to 1.0 wt%. Darkest shading is 0.1 GPa, then 0.05 GPa, and lightest
574 shading is 0.02 GPa. Liquidus temperatures expected for lunar granites are estimated to be 900 −
575 990 °C (Tuttle and Bowen, 1958; Jolliff et al., 1999), and is highlighted by the gray box. Under
576 anhydrous conditions, however, our experimental range is 950 – 1040 °C, which is based on our
577 modeling results, and is outlined by the black box.
578

Figure 3. Variation diagrams as a function of the degree of melt remaining; comparing average residual glass compositions of experimental data and rhyolite-MELTS modeled data. **Black** points are monzogabbro and **grey** points are alkali gabbronorite. **Solid lines** are experimental data and **dashed lines** are rhyolite-MELTS data. To differentiate between Si-rich and Fe-rich experimental data, **square symbols** are Si-rich data and **diamond symbols** are Fe-rich data. Rhyolite-MELTS data ranges in temperature from 1200 - 900 °C, in 50 °C increments (monzogabbro stays completely molten until <1150 °C). To reduce clutter, rhyolite-MELTS temperatures are listed on the first graph and experimental temperatures are listed on the second graph, to the right.

Figure 4. Variation diagrams showing average values for glass compositions for experiments held at 1050 and 1000 °C. **Black** symbols are monzogabbro and **gray** symbols are alkali gabbronorite. **Diamonds** are experiments carried out at 1050 °C, **circles** are experiments held at 1000 °C, and **triangles** are starting compositions. **Stars** represent a calculated intermediate glass for experiments with two immiscible liquids. **White triangles** are lunar granite bulk rock compositions.

Figure 5. BSE images of Th-doped monzogabbro and alkali gabbronorite experiments. **(a)** Monzogabbro experiment at 1050 °C. Image depicts both a dendritic crystalline texture and heterogeneities within the glass. Arrows point to the BSE-bright and -dark colored glasses. **(b)** Monzogabbro experiment held at 1000 °C, shows the sharp boundary between the two immiscible melts. **(c)** Alkali gabbronorite experiment held at 1000 °C, shows the two immiscible melts.

612 **Table 1.** Starting compositions for equilibrium crystallization experiments

Oxide (wt.%)	Monzogabbro (14161,7069)	Alkali gabbronorite (67975,117)	KREEP basalt (15386,19)
SiO_2	54.0	51.18	51.41
TiO_2	2.42	0.64	2.26
Al_2O_3	12.69	16.5	14.98
Cr_2O_3	0.05	0.09	0.31
FeO	14.1	11.8	10.68
MnO	0.2	0.18	0.16
MgO	2.7	8.3	8.27
CaO	9.07	9.1	9.82
Na_2O	1.42	0.31	0.74
K_2O	1.61	1.9	0.68
P_2O_5	1.73	0	0.71
Total	100.0	100.0	100.0

613

614

615

616 **Table 2.** Microbeam settings that were used at each institution for analysis. A Cameca MBX
617 electron microprobe was used at NAU, a Cameca SX100 and a JEOL 8530F microprobe were
618 used at JSC, and a Cameca SX100 at U of A.

	NAU	**JSC**	**U of A**
Beam current for glass (nA)	10	20	20
Beam current for minerals (nA)	20	20	40
Beam size for glass (μm)	10	10,1	5
Beam size for minerals (μm)	10	1	0
Voltage (keV)	15	15	15

619

620

621

622

623

This is a preprint, the final version is subject to change, of the American Mineralogist (MSA)
Cite as Authors (Year) Title. American Mineralogist, in press.
(DOI will not work until issue is live.) DOI: http://dx.doi.org/10.2138/am-2016-5619

624 **Table 3.** Glass and mineral compositions from equilibrium crystallization experiments

Sample	Monzogabbro													
T (°C)	1050							1000						
Phase	Gl int (23)[a]	Gl Si (20)	Gl Fe (15)	Plag (20)	Si-ph (18)	Ox (9)	Ol (3)	Gl Si (10)	Gl Fe (8)	Plag (4)	Low-Ca px (4)	Si-ph (2)	Merrill (5)	Ox (1)
SiO_2	52.6 (3.4)[b]	53.7 (0.9)	47.9 (0.6)	51.8 (0.8)	96.8 (1.5)	0.1 (0)	33.6 (0.3)	68.3 (2.3)	44.0 (0.43)	52.0 (1.17)	48.2 (0.19)	97.1 (0.3)	1.8 (1.7)	0.16
TiO_2	2.91 (0.5)	2.64 (0.1)	3.53 (0.1)	0.09 (0.02)	0.01 (0.03)	22.9 (0.8)	0.09 (0.0)	1.05 (0.1)	3.31 (0.0)	0.09 (0.02)	1.02 (0.26)	0.28 (0.04)	0.13 (0.17)	51.4
Al_2O_3	10.6 (0.7)	11 (0.11)	9.56 (0.15)	29.2 (0.4)	1.33 (0.31)	4.94 (0.3)	0.04 (0.0)	11.1 (0.56)	8.49 (0.15)	29.6 (0.9)	1.76 (0.74)	0.86 (0.81)	0.26 (0.35)	0.18
Cr_2O_3	0.04 (0.01)	0.03 (0.01)	0.04 (0.01)	0.01 (0.01)	0 (0)	15.6 (1.2)	0.06 (0.01)	0.01 (0.0)	0.03 (0.01)	0 (0)	0.28 (0.08)	0.01 (0.02)	0.01 (0.01)	0.66
FeO	17.5 (2.4)	16.2 (0.5)	20.9 (0.32)	0.68 (0.09)	0.24 (0.31)	51.9 (0.7)	43.5 (0.1)	0.9 (0.1)	23.0 (0.38)	0.9 (0.1)	29.7 (2.65)	0.3 (0.05)	4.33 (0.8)	43.7
MnO	0.28 (0.05)	0.26 (0.03)	0.35 (0.02)	0.01 (0.01)	0.02 (0.02)	0.4 (0)	0.56 (0.03)	0.01 (0.0)	0.36 (0.03)	0.01 (0.0)	0.53 (0.05)	0 (0)	0.11 (0.02)	0.41
MgO	3.32 (0.19)	3.1 (0.1)	4 (0.1)	0.19 (0.03)	0 (0.1)	3.24 (0.05)	20.5 (0.1)	0.16 (0.06)	1.91 (0.06)	0.16 (0.06)	13.34 (1.56)	0.02 (0.03)	2.06 (0.03)	1.59
CaO	7.5 (0.6)	7.4 (0.2)	8.38 (0.11)	14.2 (0.03)	0.15 (0.06)	0.15 (0.06)	0.28 (0.02)	13.73 (0.69)	9.24 (0.06)	13.73 (0.69)	3.87 (0.17)	0.16 (0.16)	41.3 (1.2)	0.19
Na_2O	1.19 (0.19)	1.3 (0)	0.93 (0.04)	2.85 (0.18)	0 (0)	0 (0)	0.0 (0)	3.18 (0.31)	0.80 (0.05)	3.18 (0.31)	0.04 (0.01)	0.15 (0.21)	0.13 (0.03)	0.0
K_2O	1.17 (0.3)	1.21 (0.1)	0.71 (0.04)	0.18 (0.03)	0.1 (0)	0.1 (0)	0.0 (0)	0.29 (0.08)	1.02 (0.05)	0.29 (0.08)	0 (0)	0.03 (0.01)	0.01 (0.0)	0.04
P_2O_5	1.97 (0.4)	1.73 (0.12)	2.45 (0.21)	0.07 (0.03)	0.03 (0.02)	0.03 (0.02)	0.95 (0.44)	0.07 (0.01)	3.62 (.07)	0.07 (0.01)	0.06 (0.03)	0 (0)	42.07 (1.46)	0.0
Th_2O	0.69 (0.16)	0.64 (0.06)	0.87 (0.07)	0.25 (0.25)	0.0 (0.01)	0.0 (0.01)	0.03 (0.05)	0 (0)	2.72 (0.25)	0 (0)	0 (0)	0.01 (0.01)	7.16 (0.15)	0.0
Total	99.69	99.23	99.63	99.25	99.5	99.3		98.8	98.5	100.3	98.8	98.0	99.32	98.3
Phase modal %		25	36.5	23	13.5	1	1	21	21	22	16	17	2	< 1

625

626

627

Sample	Alkali Gabbronorite															
T (°C)	1100				1050					1000						
Phase	Gl (17)	Plag (18)	Low-Ca px (18)	Ol (11)	Gl (5)	Plag (2)	Low-Ca px (4)	Ol (4)	Thor (1)	Gl Si (8)	Gl Fe (7)	Plag (1)	Low-Ca px (13)	Ol (23)	Ilm (3)	Thor (5)
SiO_2	59.1 (0.8)	47.5 (1.0)	51.9 (0.4)	37.4 (0.25)	62.4 (1.37)	48.0 (0.91)	49.7 (0.5)	36.0 (0.6)	19.1	71.7 (2.17)	46.0 (4.0)	47.7	51.5 (0.85)	37.3 (1.42)	3.63 (1.07)	20.7 (2.08)
TiO_2	1.5 (0.1)	0.04 (0.03)	0.43 (0.11)	0.04 (0.02)	1.96 (0.09)	0.03 (0.0)	0.43 (0.1)	0.02 (0.01)	0.06	1.1 (0.10)	6.15 (1.02)	0.05	0.36 (0.11)	0.03 (0.02)	32.2 (0.43)	0.09 (0.07)
Al_2O_3	11.6 (0.2)	30.6 (0.6)	1.54 (0.4)	0.09 (0.15)	11.3 (0.14)	32.3 (0.62)	1.44 (0.8)	0.02 (0.0)	0.57	11.0 (0.50)	6.85 (0.55)	32.0	2.85 (1.47)	0.12 (0.27)	2.11 (0.34)	0.66 (0.53)
Cr_2O_3	0.02 (0.01)	0.01 (0.01)	0.32 (0.12)	0.07 (0.02)	0.02 (0.01)	0 (0)	0.14 (0.04)	0.08 (0.03)	0.0	0 (0)	0 (0)	0.0	0.34 (0.17)	0.07 (0.03)	0.06 (0.03)	0 (0)
FeO	11 (0.7)	1.5 (0.2)	22.2 (1.1)	30.1 (0.9)	9.35 (1.0)	0.71 (0.18)	26.2 (1.23)	30.4 (3.26)	1.32	6.63 (1.32)	26.0 (2.32)	0.78	19.9 (4.71)	28.2 (7.19)	58.3 (0.80)	1.39 (0.24)
MnO	0.15 (0.03)	0.02 (0.02)	0.44 (0.04)	0.33 (0.03)	0.13 (0.01)	0 (0)	0.42 (0.04)	0.32 (0.04)	0.03	0.07 (0.02)	0.33 (0.03)	0.05	0.36 (0.09)	0.29 (0.07)	0.37 (0.03)	0.01 (0.01)
MgO	2.4 (0.1)	0.45 (0.08)	18.7 (1.1)	32.8 (0.9)	1.38 (0.16)	0.42 (0.01)	16.4 (1.0)	32.3 (2.6)	0.0	0.16 (0.05)	0.68 (0.06)	0.4	20.4 (3.86)	33.0 (6.14)	0.64 (0.20)	0.01 (0.01)
CaO	7.1 (0.3)	17.3 (0.4)	4.67 (0.8)	0.28 (0.08)	5.8 (0.52)	17.3 (0.6)	3.73 (0.45)	0.21 (0.02)	0.23	3.09 (0.51)	8.34 (0.96)	17.3	3.44 (1.19)	0.23 (0.09)	0.31 (0.11)	0.26 (0.10)
Na_2O	0.45 (0.02)	0.79 (0.9)	0.03 (0.1)	0 (0)	0.38 (0.02)	0.81 (0.09)	0 (0)	0 (0)	0.01	0.28 (0.02)	0.14 (0.03)	0.93	0.01 (0.01)	0.01 (0.01)	0 (0)	0.02 (0.02)
K_2O	3.3 (0.3)	0.38 (0.08)	0.03 (0.06)	0.01 (0.01)	3.76 (0.45)	0.32 (0.09)	0.01 (0.01)	0 (0)	0.0	5.56 (0.17)	1.42 (0.64)	0.4	0.01 (0.01)	0.01 (0.01)	0.31 (0.16)	0.20 (0.26)
P_2O_5	0.02 (0.02)	0.03 (0.02)	0.01 (0.01)	0.02 (0.02)	-	-	-	-	0.01	-	0.08 (0.03)	-	0.01 (0.01)	0.04 (0.04)	0.04 (0.02)	0.08 (0.02)
Th_2O	1.62 (0.14)	0.02 (0.03)	0.02 (0.04)	0.01 (0.02)	0.83 (0.13)	0 (0)	0.01 (0.01)	0 (0)	52.08	0.32 (0.07)	3.80 0.44)	0.01	0.01 (0.01)	0.01 (0.01)	1.49 (2.51)	75.7 (1.67)
Total	98.4	98.2	100.3	101.26	97.4	99.8	98.4	99.43	73.5	99.9	100.6	99.6	99.2	99.35	99.5	99.1
Phase modal %		48.5			26	42	28		< 1	< 5	< 5	44				

628

629

Sample	KREEP basalt			
T (°C)	1100 °C			
Phase	Gl (37)	Plag (17)	Low-Ca px (44)	Sp (11)
SiO_2	52.3 (0.4)	48.1 (0.7)	53.6 (0.7)	0.12 (0.01)
TiO_2	3.12 (0.2)	0.08 (0.02)	0.63 (0.12)	1.88 (0.23)
Al_2O_3	12.6 (0.4)	30.7 (0.5)	2.86 (0.56)	18.1 (0.6)
Cr_2O_3	0.11 (0.02)	0 (0)	0.65 (0.09)	44.7 (1.5)
FeO	12.0 (0.2)	0.57 (0.07)	13.5 (0.8)	26.4 (0.3)
MnO	0.18 (0.03)	0.02 (0.01)	0.26 (0.03)	0.24 (0.02)
MgO	5.42 (0.12)	0.37 (0.04)	26.8 (0.6)	7.75 (0.12)
CaO	9.50 (0.13)	16.5 (0.3)	2.11 (0.14)	0.16 (0.05)
Na_2O	0.68 (0.03)	1.38 (0.1)	0.01 (0.01)	0.01 (0.01)
K_2O	0.59 (0.02)	0.1 (0.02)	0 (0)	0 (0)
P_2O_5	0.98 (0.11)	0.04 (0.02)	0.03 (0.03)	0.01 (0.01)
Th_2O	0.88 (0.07)	0.02 (0.04)	0.02 (0.02)	-
Total	98.3	97.9	100.3	99.4
Phase modal %	69	11	20	<1

630

631 ***a** represents number of analyses that were taken using the electron microprobe, **b** represents the standard deviation. Gl = glass, Int =
632 intermediate glass, Si = silica-rich glass, Fe = FeO-rich glass. Plag = plagioclase. Si-ph = Silica polymorph. Ol = olivine. Low-Ca px =
633 low-Ca pyroxene. Thor = thorite. Ilm = ilmenite. Merrill = Merrillite. Sp = spinel.

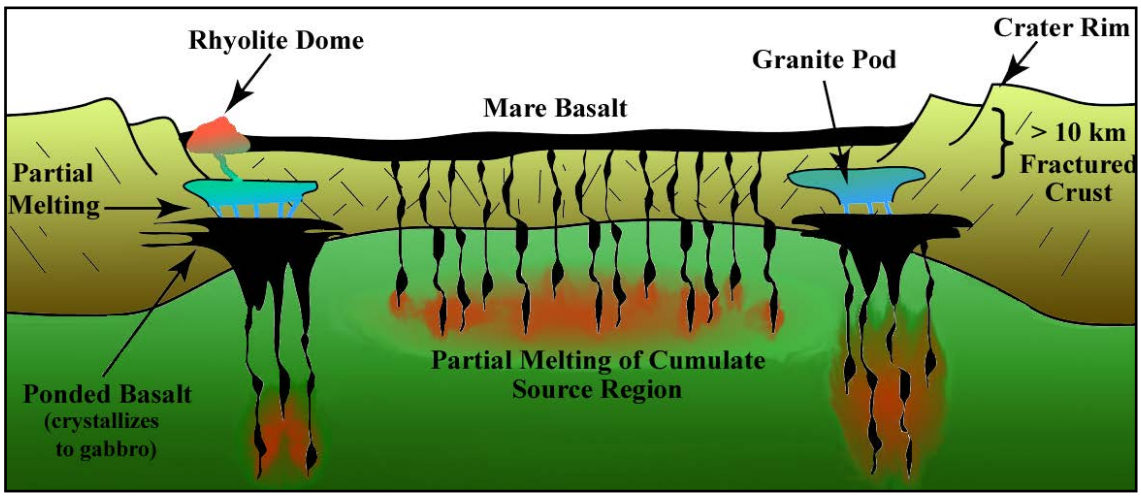
Rhyolite Dome
Crater Rim
Granite Pod
Mare Basalt
> 10 km
Fractured
Crust
Partial
Melting
Partial Melting of Cumulate
Source Region
Ponded Basalt
(crystallizes
to gabbro)

Figure 1.

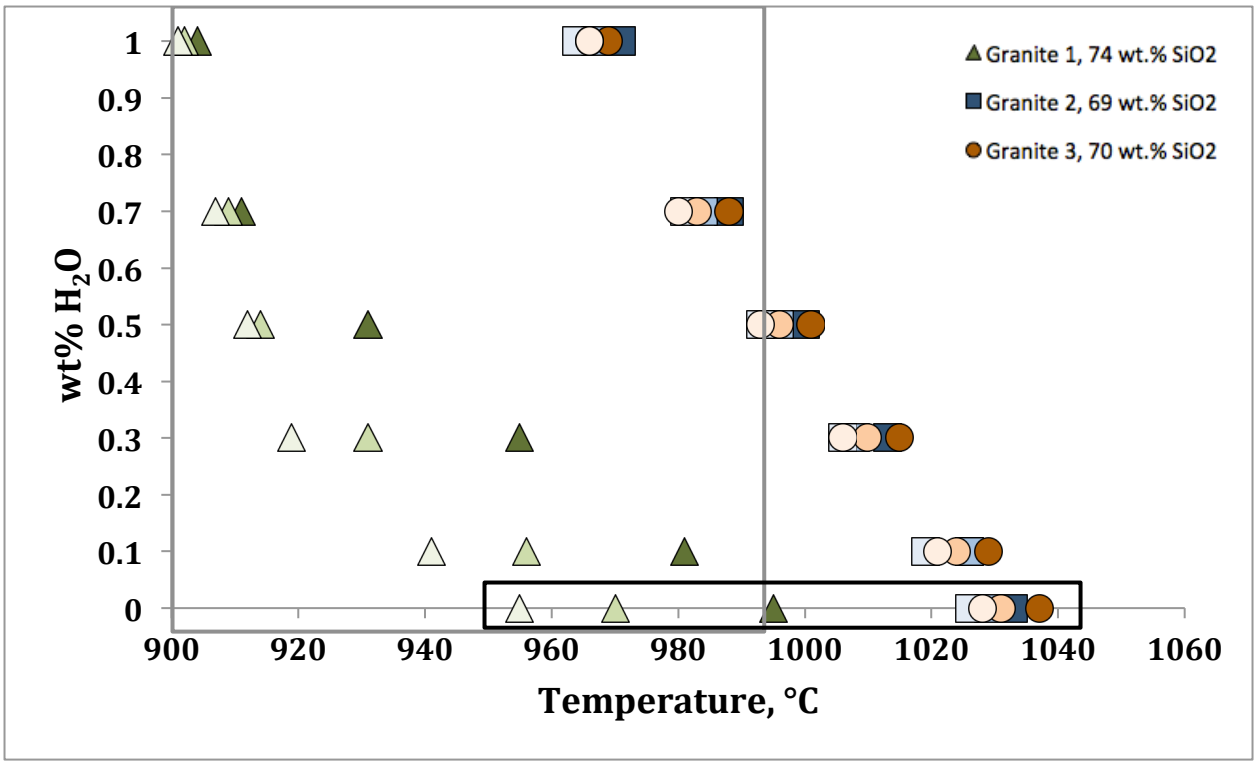

Figure 2. Lunar granite liquidus diagram.

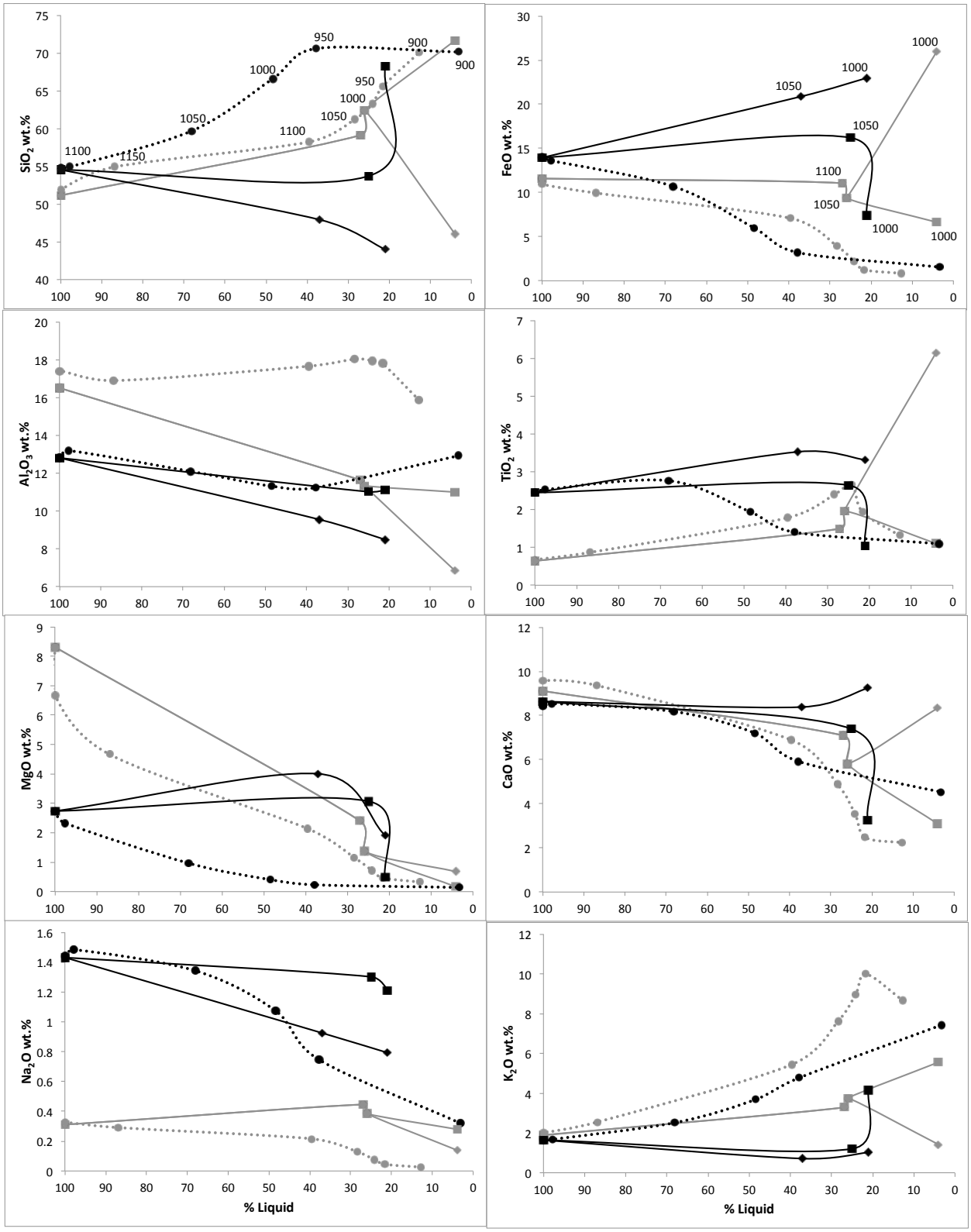

Figure 3. Variation diagrams of experimental and modeling residual glass data.

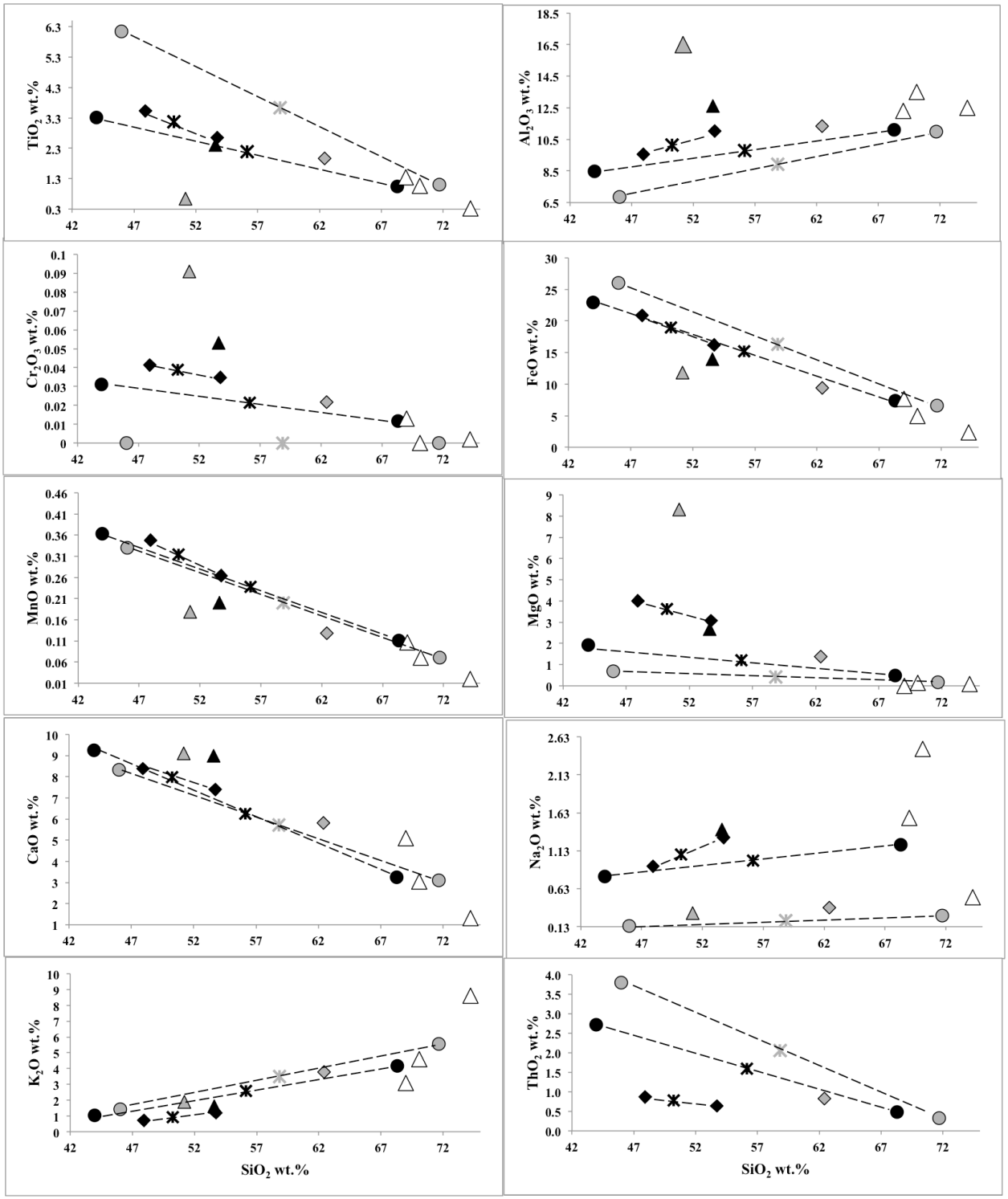
TiO2 wt.%
Al2O3 wt.%
Cr2O3 wt.%
FeO wt.%
MnO wt.%
MgO wt.%
CaO wt.%
Na2O wt.%
K2O wt.%
ThO2 wt.%
SiO2 wt.%
SiO2 wt.%

Figure 4.

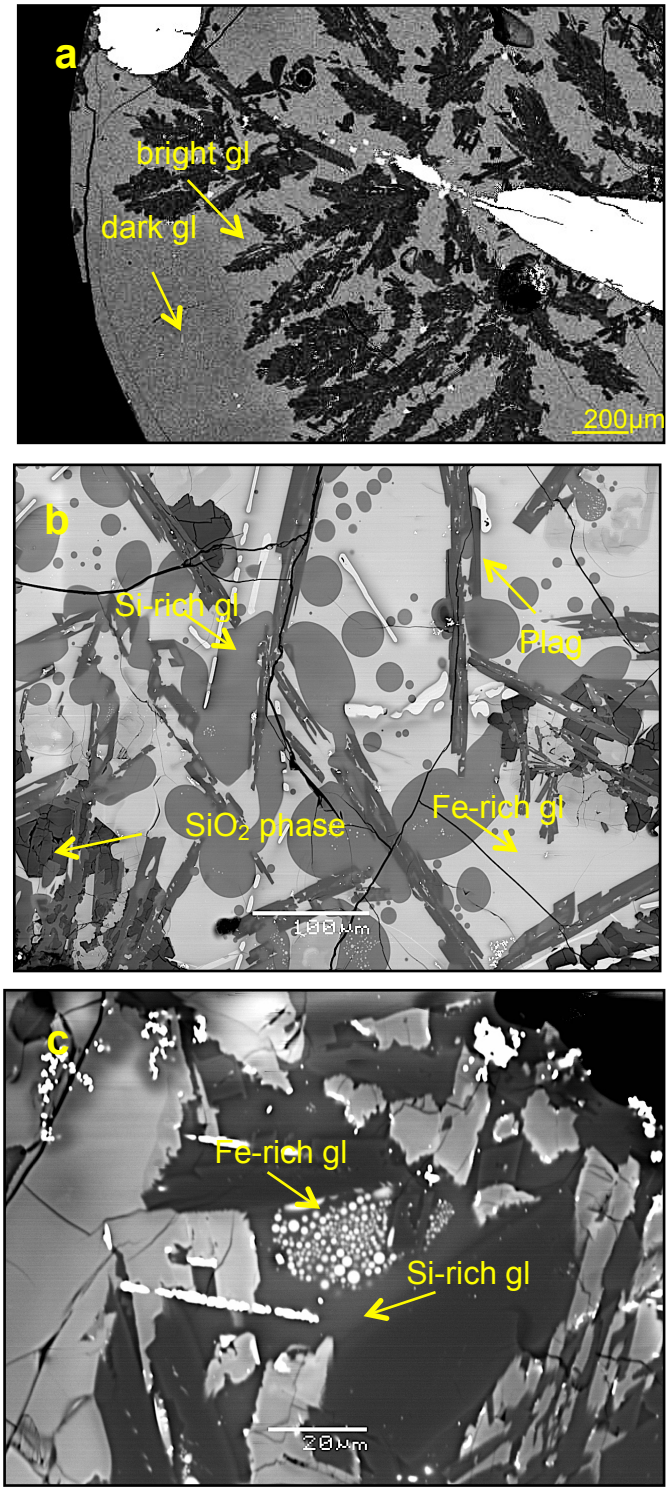
a
bright gl
dark gl
200µm
b
Si-rich gl
Plag
SiO2 phase
Fe-rich gl
100µm
c
Fe-rich gl
Si-rich gl
20µm

Figure 5.